

Alma Mater Studiorum Università di Bologna
Archivio istituzionale della ricerca

Combining the highest degradation efficiency with the lowest environmental impact in zinc oxide based photocatalytic systems

This is the final peer-reviewed author's accepted manuscript (postprint) of the following publication:

Published Version:

Costamagna M., Ciacci L., Paganini M.C., Calza P., Passarini F. (2020). Combining the highest degradation efficiency with the lowest environmental impact in zinc oxide based photocatalytic systems. JOURNAL OF CLEANER PRODUCTION, 252, 1-9 [10.1016/j.jclepro.2019.119762].

Availability:

This version is available at: <https://hdl.handle.net/11585/714222> since: 2023-05-25

Published:

DOI: <http://doi.org/10.1016/j.jclepro.2019.119762>

Terms of use:

Some rights reserved. The terms and conditions for the reuse of this version of the manuscript are specified in the publishing policy. For all terms of use and more information see the publisher's website.

This item was downloaded from IRIS Università di Bologna (<https://cris.unibo.it/>).
When citing, please refer to the published version.

(Article begins on next page)

This is the final peer-reviewed accepted manuscript of:

Costamagna M.; Ciacci L.; Paganini M.C.; Calza P.; Passarini F., Combining the highest degradation efficiency with the lowest environmental impact in zinc oxide based photocatalytic systems, «JOURNAL OF CLEANER PRODUCTION», 2020, 252, Article number: 119762, pp. 1 - 9.

The final published version is available online at:
<https://dx.doi.org/10.1016/j.jclepro.2019.119762>

Terms of use:

Some rights reserved. The terms and conditions for the reuse of this version of the manuscript are specified in the publishing policy. For all terms of use and more information see the publisher's website.

This item was downloaded from IRIS Università di Bologna (<https://cris.unibo.it/>)

When citing, please refer to the published version.

Combining the Highest Degradation Efficiency with the Lowest Environmental Impact in Zinc Oxide Based Photocatalytic Systems

Mattia Costamagna¹, Luca Ciacci^{2*}, Maria Cristina Paganini¹, Paola Calza^{1*}, Fabrizio Passarini^{2,3}

¹Department of Chemistry, University of Turin, Via P. Giuria 7, 10125 Torino, Italy

²Department of Industrial Chemistry “Toso Montanari”, University of Bologna, Viale del Risorgimento 4,
40136 Bologna, Italy

³Interdepartmental Centre for Industrial Research “Renewable Resources, Environment, Sea and Energy”,
University of Bologna, Via D. Campana 71, 47922, Rimini

*Corresponding author – LC: +39.0541.434483 Telephone; +39.0541.434480 Facsimile

E-mail address: luca.ciacci5@unibo.it

*Corresponding author – PC: +39.011.6705268 Telephone; +39.011.6705242 Facsimile

E-mail address: paola.calza@unito.it

This item was downloaded from IRIS Università di Bologna (<https://cris.unibo.it/>)

When citing, please refer to the published version.

Highlights

- The removal of organic pollutants from wastewater by heterogeneous photocatalysis is explored
- Zinc oxide photocatalysts doped with rare earth elements are employed
- Design of experiments and life cycle assessment are combined to heterogeneous photocatalysis
- The highest degradation efficiency is obtained with 1700 mgL⁻¹ of cerium-doped zinc oxide
- A concentration of 800 mgL⁻¹ is preferable to reduce the overall environmental impact

Abstract

Heterogeneous photocatalysis may diversify and augment access to unconventional water sources like wastewater. However, the energy embodied in water treatment and supply in photocatalytic systems make process efficiency considerations and environmental impacts assessment of primary relevance towards the setting of sustainable strategies. In this work, we evaluated the degradation rate of phenol in water by using different photocatalysts based on zinc oxide doped with rare earth elements. Aiming at identifying the best operating conditions that couple the highest degradation efficiency with the lowest environmental burdens, the results of an experimental design face centred model were combined to life cycle assessment. Based on previous works of the authors, the concentration of photocatalyst, type of rare earths used as dopant, its precursor and dopant concentration in the photocatalyst constituted the set of explanatory variables. Cumulative energy demand and IPCC 2013 GWP 100y were used as life cycle impact assessment methods. The results show that the highest degradation efficiency is obtained with 1700 mgL⁻¹ of cerium-doped zinc oxide from nitrate precursor. However, setting the photocatalyst concentration at 800 mgL⁻¹ may be preferable to reduce the overall environmental impact, mainly associated with the input of electrical energy and the synthesis of the material. Advanced oxidation processes like the heterogeneous photocatalytic process investigated in this study are promising ways to achieve high standards of wastewater purification and environmental protection. To this aim, the chance of exploiting the solar light to promote photocatalysis and the possibility to hold the catalyst on supports that may facilitate its recovery for regeneration are of great interest to scale this technique up to real systems at lower economic and environmental cost.

Keywords: zinc oxide; rare earth elements; life cycle assessment; DoE; wastewater; photocatalysis

This item was downloaded from IRIS Università di Bologna (<https://cris.unibo.it/>)

When citing, please refer to the published version.

1. Introduction

Water scarcity will be among the most urgent global emergencies to face in the next decade (Liu et al., 2015; World economic forum, 2018). This problem is expected to affect about two-thirds of the world's population and, at the same time, the constant decline of water quality, the over-exploitation of water basins and increasingly violent climate events (floods, droughts) will exacerbate conflicts and poverty (Capocelli et al., 2019). Guaranteeing water access, responsible and sustainable water management to all is mainstreamed in several sustainable development goals SDGs, and research is ongoing to find ways of augmenting water sources including, for instance, reuse, desalination of seawater and wastewater remediation (Bolisetty et al., 2019; Mehta et al., 2015; Asadollahi et al., 2017; Warsinger et al., 2018). In regard to the latter points, however, some concerns have risen, respectively, on the increase in the energy required to supply water from alternative sources due to the interlinkages in the water-energy nexus (Sovacool, B.K. and Sovacool, K.E., 2009; Mo et al., 2014; Mekonnen et al., 2015; Gjorgiev, B. and Sansavini, 2017; Larsen and Drews, 2019; Friedrich, 2002; Stokes and Horvath, 2006) as well as on the provisioning of safe water and contaminant abatement (Ortiz et al., 2016; Dirk van der Kooij and van der Wielen, 2014; Homem and Santos, 2011). Of more interest here, heterogeneous photocatalysis has a great potential to be a cost-effective water purification technology (Lee et al., 2015) for the removal of low concentration recalcitrant organic pollutants from wastewater. Among the semiconductor oxides, titanium dioxide and zinc oxide are the most promising candidates (Lee et al., 2015), particularly when the latter system is doped with rare earth elements (REEs) such as cerium (Ce), lanthanum (La), praseodymium (Pr), erbium (Er) and ytterbium (Yb) (Calza et al., 2017; Sordello et al., 2019).

Beyond catalysis, REEs' unique physical and chemical properties are increasingly important in several hi-tech applications such as clean energy technologies, hybrid vehicles, pollution control, optics, and refrigeration (Koltun and Tharumarajah, 2014). However, an interconnected mine extraction route and imbalances between production and demand might cause future supply disruption for some REEs (e.g., neodymium and dysprosium) or oversupply and consequent material stockpiling for other REEs (e.g., La, Ce) with a cascade effect in their market price (Ciacci et al., 2019). Moreover, primary production of REEs is far from being environmentally sustainable as it requires considerable inputs of materials and energy, and it generates large quantities of emissions and solid waste (Navarro and Zhao, 2014). Therefore, analytical tools and strategies aiming at optimizing the use of REEs in common applications would result in the combined effect of increasing their functionality in use while minimizing the associated environmental implications.

Alone or in combination with quantitative assessment methodologies, life cycle assessment (LCA) has been often the preferred technique to evaluate the environmental performance of products and processes. In the past years, LCA has been extensively applied to water management and water treatment systems (Rodríguez-

This item was downloaded from IRIS Università di Bologna (<https://cris.unibo.it/>)

When citing, please refer to the published version.

Garcia et al., 2011; Pasqualino et al., 2011; Meneses et al., 2010; De Faria et al., 2015; Morera et al., 2016; Sabeen et al., 2018) supporting decision-makers in the development of water strategies and frameworks (Díaz-Madronero et al., 2018; Krozer et al., 2010; Garrone et al., 2018; Capocelli et al., 2019; Ramírez et al., 2019).

Similarly, LCA has been applied to unveil the potential environmental benefits resulting from REEs reuse and recycling practices (Schulze et al., 2018; Sprecher et al., 2014; Zakotnik et al., 2016; Nuss and Eckelman, 2014; Binnemans et al., 2013; Yang et al., 2016; Ciacci et al., 2019). While these studies have contributed to increase understanding and awareness on the need to address sustainability in anthropogenic systems, they have seldom included a systematic evaluation of operating parameters and set the best system conditions for achieving optimal process efficiency and environmental sustainability. In this sense, the design of experiments (DoE) enables to explore and set the best experimental conditions with a relatively small number of experiments. Compared to traditional one-variable-at-time (OVAT) approach, DoE can extend the investigated domain to the interactions among experimental variables, which would be otherwise out of the reach with the conventional OVAT approach. When combined to DoE, LCA has a potential for providing a quantitative environmental assessment of different solutions and strategies.

The potential for integrating DoE and LCA was explored in this study. The use of REEs-doped ZnO catalysts for the photoinduced degradation of pollutants in contaminated water was selected as a case study with the aim of identifying the optimal system conditions that combine the highest degradation efficiency with the lowest greenhouse gas (GHG) emissions and energy use.

2. Materials and methods

In previous works, pure and Ce-doped ZnO catalysts were utilised to investigate the degradation of phenol and several refractory compounds in ultrapure water at natural pH and under UV-Vis light conditions (Calza et al., 2017). The hydrothermal route was followed to prepare the catalytic systems from different precursors. This production route complies with the Green Chemistry principles and enables to obtain controlled nanostructures. The synthesized bare ZnO catalysts and those doped with REEs were characterized by means of scanning electron microscopy, transmission electron microscopy, X-rays diffraction, UV visible diffuse reflectance spectroscopy, electron paramagnetic resonance, chronopotentiometry, and cyclic voltammetry (Calza et al. 2017; Cerrato et al., 2018; Sordello et al., 2019). The synthesized materials resulted particularly promising so that in a subsequent study the investigation was extended to other dopants, namely Er and Yb (Sordello et al., 2019). These studies constituted the basis on which the DoE model was built and applied to a systematic investigation of the photocatalytic degradation of phenol in water solution in presence of ZnO photocatalysts doped with Ce, Er, and Yb.

This item was downloaded from IRIS Università di Bologna (<https://cris.unibo.it/>)

When citing, please refer to the published version.

2.1 Experimental design

Overall, the photocatalytic reaction may depend on several operating parameters such as phenol concentration, concentration of the photocatalyst, type and concentration of dopant elements, pH of water solution, size, structure, and surface area of the photocatalyst, reaction temperature, presence of inorganic ions, presence of oxygen, wavelength and irradiation time (Kumar and Pandey, 2017; Márquez et al., 2012; Reza et al., 2017). However, the type and concentration of dopant in the photocatalyst (X_1) and the concentration of the catalytic system in solution (X_2) were set as the only factors of interest in DoE. The choice to focus only on these two parameters was based on the results obtained in previous studies (Calza et al., 2017; Sordello et al., 2019) and the experience of the practitioners.

A faced centered design (FCD) model was utilised to determine linear and quadratic effect of X_1 and X_2 as well as interactions between X_1 and X_2 . In FCD, a full factorial, a star design, and N replicates of the center points are modelled. Three levels (-1 , 0 , $+1$) were set for each variable (Table 1) based on concentration ranges derived from previous experiments. The three REEs (i.e., Ce, Er, and Yb) used as dopants of ZnO are treated as qualitative variables in FCD. Thus, the total number of experiments (N) for each doping element is computed as follows:

$$N = 2^f + 2f + N_0 \quad (\text{eq. 1})$$

Where f is the number of variables and N_0 is the number of replicates in the centre points. Setting $f = 2$ and $N = 2$ respectively, the total number of experiments is 20 or 10 for each precursor (i.e., chloride and nitrate). However, the subset of experiments for X_1 at level -1 , which correspond to bare ZnO photocatalyst, is common to both precursors. Thus, for each REEs investigated, the resulting total number of independent experiments reduced to 17 with two replicates of experiments in the centre.

The mathematical model resulting from the FCD is in the form:

$$Y = B_0 + B_1X_1 + B_2X_2 + B_{11}X_{12} + B_{22}X_{22} + B_{12}X_1X_2 \quad (\text{eq. 2})$$

Where Y is the calculated response (the reaction rate constant k), X_1 is the dopant concentration in the photocatalyst, X_2 is the concentration of the catalytic system employed in the degradation process, B_0 is the constant, B_1 is the coefficient of the linear effect of X_1 , B_2 is the coefficient of the linear effect of X_2 , B_{11} is the coefficient of the quadratic effect of X_1 , B_{22} is the coefficient of the quadratic effect of X_2 , B_{12} is the coefficient of the interaction effect between X_1 and X_2 .

Table 1. Variables, investigated levels and their actual values utilised in the design of experiments.

This item was downloaded from IRIS Università di Bologna (<https://cris.unibo.it/>)

When citing, please refer to the published version.

The experiments were randomized to avoid external influence on the results and elaborated with the Chemometric Agile Tool (CAT) software (Gruppo di Chemiometria, 2019). The full experimental matrix for the FCD model created is reported in the Supporting Information (Table S1).

| Variable | | | Level | | |
|----------------|----------------------------------|-------------------|-------|-----|------|
| # | Description | Unit | -1 | 0 | +1 |
| X ₁ | Rare earth element concentration | % w/w | 0 | 0.5 | 1 |
| X ₂ | Photocatalyst concentration | mgL ⁻¹ | 100 | 800 | 1500 |

2.2 Experimental section

A bare ZnO sample was synthesized starting from a water solution of Zn(NO₃)₂·6H₂O (1 M). Then, NaOH (4 M) was added dropwise until the pH was 10-11. The solution was transferred into a 100 mL PTFE lined stainless steel autoclave (occupying 70% of the effective volume) and then treated at 175°C overnight. The product was centrifuged, washed with deionized water, and dried at 70°C.

The ZnO samples doped with REEs (0.01 M) were prepared by adding stoichiometric amounts of Ce, Er, and Yb to the starting solution. The precursor salts employed were respectively CeCl₃·7H₂O and Ce(NO₃)₃·6H₂O for Ce, ErCl₃·6H₂O and Er(NO₃)₃·5H₂O for Er, YbCl₃·6H₂O and Yb(NO₃)₃·5H₂O for Yb. The synthesis route then followed the same procedure described above for the bare ZnO sample (Calza et al., 2017). The samples were labelled as XZp-S where X = dopant element (i.e., REE); Z = Zinc oxide; p = percentage of dopant in the photocatalysts (i.e, 0%, 0.5%, 1%); S = type of salt used for as dopant precursor (i.e., Cl or NO₃).

The photocatalytic degradation of synthesized photocatalysts was assessed using 60 mgL⁻¹ of phenol as a probe molecule. Phenol was chosen as an indicator substance representative for the groups of phenolic compounds, which are common pollutants in industrial wastewater streams. Phenol is soluble in water and relatively stable in the environment, so as specific treatments to remove or degrade it are required (Chiou and Juang, 2007).

Samples were load into cylindrical Pyrex cells (4.0 cm diameter and 2.5 cm height, cut-off at 295 nm) filled with 5 mL of an aqueous suspension containing phenol and the photocatalyst powder at selected concentrations. Samples were subjected to different irradiation times (ranging from 5 min to 3 h), using a set of six Actinic BL TL-D 15W (Phillips, Eindhoven, Nederland). The spectral region extended from 340 to 410 nm, with a maximum centred at 370 nm and a narrow band centred at 435 nm. The UV integrated irradiance on the cells in the 290–400 nm range wavelengths was 35 ± 1 Wm⁻² (lamps emission spectra and incident irradiance were recorded with a calibrated spectrum radiometer, Ocean Optics SD2000 CCD

This item was downloaded from IRIS Università di Bologna (<https://cris.unibo.it/>)

When citing, please refer to the published version.

spectrophotometer, equipped with an optic fiber and a cosine corrector CC-3-UV-T)). During irradiation, the suspensions were magnetically stirred.

After irradiation, the suspensions were filtered by means of a 0.45 μm hydrophilic PTFE membrane (Millipore Millex-LCR). All samples were analysed using a Merck-Hitachi liquid chromatographer equipped with a Rheodyne injector L-6200 and L-6200A pumps for high-pressure gradients, a L-4200 UV-Vis detector (the detection wavelength was set at 220 nm) and a column LiChrocart RP-C18 (Merck, 12.5 cm x 0.4 cm). Elution was carried out at 1 mL min⁻¹ with 4.2 mM aqueous H₃PO₄:CH₃CN 70:30 in isocratic mode. The injection volume was 50 μL .

With the exception of Carlo Erba's phosphoric acid (pure at 85%), all the reactants were purchased from Sigma-Aldrich with purity higher than 99.9% and were used without any further purification. HPLC grade water was obtained from MilliQ System Academic (Waters, Millipore).

2.3 Assessment of environmental impacts

LCA enables the assessment of the environmental impacts associated with a product, a process or a service along its entire life cycle. According to ISO 14040 and 14044, LCA consists of four phases including goal and scope definition, life cycle inventory (LCI), life cycle impact assessment (LCIA), and results interpretation (ISO, 2006a; ISO, 2006b).

The goal and scope definition sets the object of the study, the system boundaries and the functional unit. As mentioned above, the aim of this study is to evaluate and compare the efficiency of different photocatalysts that can be used for the degradation of organic pollutants in water streams. The term efficiency refers here to the degradation rate of phenol and the environmental performance attributable to the photocatalytic systems. The reaction constant (k) to complete degradation of 60 mgL⁻¹ of phenol in MilliQ water was set as the functional unit and measured in min⁻¹. All the steps for the preparation of the photocatalysts and the degradation process were included in the system boundaries. Infrastructure and equipment used during the experimental analysis were excluded from calculation as well as the transport of direct input materials because their impact is expected to be marginal.

An inventory of inputs and outputs was compiled to create a representative model of the system under scrutiny (see Figure 1). LCI of material and energy flows for the synthesis of the precursors and for carrying the photodegradation out was modelled from direct measurements in the laboratory. Instead, literature dataset were used to model the production of rare earth oxide (REO) and the synthesis of the precursors. More in detail, REEs extraction is mainly carried out in China (Hellman and Duncan, 2014) via either open-pit mining of bastnäsite and monazite minerals or leaching of ion-adsorption clays. The Ecoinvent process “Rare earth concentrate, 70% REO, from bastnäsite, at beneficiation” provided the initial dataset to typical

This item was downloaded from IRIS Università di Bologna (<https://cris.unibo.it/>)

When citing, please refer to the published version.

bastnäsite mining and refining in China (Althaus et al., 2007). Nuss and Eckelman (2014) updated the Ecoinvent data by re-allocating energy and materials inputs and emissions based on Bayan Obo bastnäsite composition provided in Chinese Rare-Earth Year book 2010 and 2006–2010 REO prices. It is worth noting that the bastnäsite mineral usually contains about 50% of Ce and only traces of the other two elements used as dopant in this study (i.e., Er and Yb). These two elements are part of the so-called group of heavy rare earth elements (HREEs), which are mainly extracted from ion absorption deposits (Peiró and Méndez, 2013). This production route was not investigated by Nuss and Eckelmann (2014). More integrative research in this sense is needed.

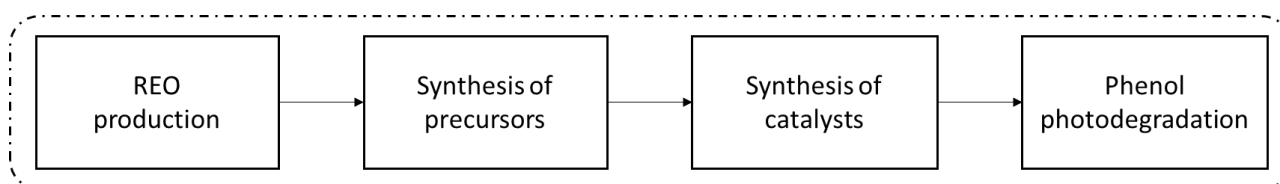


Figure 1. System layout with the main processing stages considered in the LCA model. REO – rare earth oxide.

The Ecoinvent process "*Electricity, low voltage {IT}*" was used to model the environmental impacts from the national electricity production mix, supplied to the synthesis of precursors and the photodegradation process. The inventory for the preparation of zinc nitrate hexahydrate was compiled from a patent (August, 1965). For Ce precursors, the modelling was based on information reported in Blanchard (1936) for chloride salts and in Pitts (1979) for nitrates.

The inventory for the preparation of erbium chloride was modelled according to the work of Gupta and Krishnamurthy (2005), while data for ytterbium chloride were obtained from Sebastian and Seifert (1998). For Er and Yb nitrates, the input of nitric acid was gathered from "Handbook of Chemistry and Physics" (2018) (Rumble, 2018). Instead, inputs of water, energy and the synthesis yields were set as those reported for the synthesis of zinc nitrate because of a lack of primary data. All the data employed in the model refer to the laboratory scale (see Table 2).

Table 2. Estimate of inputs of water and energy used to model the precursors' synthesis.

| Precursor | Amount (kg) | Water (l) | Energy (kWh) |
|------------------------------------------------------|-------------|-----------|--------------|
| Zn(NO ₃) ₂ ·6H ₂ O | 1 | 6.6 | 5 |
| CeCl ₃ ·7H ₂ O | 1 | 1.1 | 0.5 |
| Ce(NO ₃) ₃ ·6H ₂ O | 1 | 1.1 | 0.7 |
| ErCl ₃ ·6H ₂ O | 1 | 0.7 | 2 |
| Er(NO ₃) ₃ ·5H ₂ O | 1 | 0.85 | 0.8 |
| YbCl ₃ ·6H ₂ O | 1 | 0.7 | 2 |
| Yb(NO ₃) ₃ ·5H ₂ O | 1 | 6.6 | 5 |

LCIA aims at quantifying the environmental burdens for selected impact categories associated with a material and energy inventory. In LCA, impact categories are associated to the environmental interventions attributable to the life-cycle of a product (materials, energy used and emissions) and commonly calculated as follows:

$$IR_c = \sum_s CF_{c,s} \times m_s \quad (\text{eq. 3})$$

Where IR_c is the indicator result of the impact category c , m_s is the amount of the emission s and $CF_{c,s}$ is the characterization factor relative to an impact category c and specific for emission s (Heijungs, R. and Koning, A., 2004).

The LCIA was conducted with SimaPro 8 selecting Cumulative Energy Demand (CED) and the IPCC 2013 GWP 100y method as the impact assessment indicators. More specifically, CED accounts for gross energy requirements and includes “the direct uses as well as the indirect [...] consumption of energy due to the use of [...] raw materials”. CED indicator is split up into non-renewables and renewable energy carriers, the intrinsic value of which is determined by the amount of energy withdrawn from nature and it is expressed in MJ. (Hischier et al., 2010; Frischknecht et al., 2007)

Instead, IPCC 2013 GWP 100y is a metric for estimating the relative global warming potential (GWP) due to atmospheric emission of 1 kg of a particular greenhouse gas (GHG) compared to the emission of 1 kg of carbon dioxide (Houghton et al., 2001) over a time horizon of 100 years.

The outcomes of the inventory and of the impact assessment are following discussed to identify material and energy flows with the most significant impacts in the system.

3. Results and Discussion

The results of the photocatalytic degradation of phenol, DoE and LCA are here presented and discussed. Implications for theory and for possible industrial applications are also commented at the end of this section.

3.1 Photocatalytic degradation of phenol

This item was downloaded from IRIS Università di Bologna (<https://cris.unibo.it/>)

When citing, please refer to the published version.

Table 3 shows the DoE results for the photocatalytic degradation reaction obtained from ZnO-based materials doped with Ce, Er, and Yb and synthesized using either chloride or nitrate precursors. Overall, the presence of the REE-based dopant results in faster degradation rates than those achievable by bare ZnO photocatalyst. These findings are aligned with preliminary results (Calza et al., 2017; Sordello et al., 2019), but the FCD outcomes enabled here to investigate the entire domain of responses.

While for Ce- and Er-doped photocatalysts the choice of precursor seems not to influence the degradation rate of phenol remarkably, for Yb-doped photocatalyst a net preference is given to the nitrate salt precursor. In terms of the calculated response, the three REEs used as dopants in ZnO photocatalyst rank as follows: Ce > Yb > Er. For Ce-doped ZnO catalytic systems from nitrate precursor the relationship between the degradation rate and the investigated variables at coded scores is described by the model in eq. 4. Similar results were obtained for Er- and Yb-doped photocatalysts (see the Supporting Information).

$$Y = 0.0696 + 0.0168X_1 + 0.0412X_2 + 0.0135X_1^2 + 0.00536X_2^2 - 0.0136X_1X_2 \quad (\text{eq.3})$$

The adjusted r^2 and the standard deviation of the residuals resulted in 0.94 and 0.0092 respectively. Figure 2 shows the significance of coefficients (i.e., *: $p < 0.05$; **: $p < 0.01$; ***: $p < 0.001$) for Ce-doped ZnO photocatalyst. Both X_1 and X_2 have an effect on the photochemical degradation, but the model seems to attribute the greatest significance (marked with ***) to the concentration of the photocatalyst (i.e., X_2). The concentration of the doping REE (X_1) in ZnO has a smaller linear effect but, notably, a more significant quadratic effect (at 95% confidence) than X_2 . This evidence is detectable from the curve response surfaces of the FCD model but it cannot be deduced from the sole kinetic curves (see Figure 3), confirming the usefulness of DoE in maximizing understanding of chemical reactions. Response surfaces and significance of coefficients for all photocatalytic systems employed in the degradation process are reported in the Supporting Information (Figure S1-S2).

As early mentioned, the higher k values were observed at the maximum value of X_2 and X_1 (Table 3), with the degradation rate increasing along the diagonal of Figure 3 X_1 , implying that the effect of the photocatalyst increases at relatively high dopant concentrations. Because the best calculated responses were observed at the maximum values of X_2 and X_1 , we decided to extend the investigated domain by carrying out, respectively, one experiment at bare ZnO concentration of 2000 mgL⁻¹, and two experiments with CeZn1-Cl at 1700 mgL⁻¹ and 2000 mgL⁻¹.

The degradation curves obtained for phenol as a function of the irradiation time in ultrapure water in presence of bare and Ce-doped ZnO are plotted in Figure 4. The degradation curves for Er- and Yb-doped ZnO are instead reported in Figures S3-S5 in the Supporting Information. Panel (a) in Figure 4 shows the degradation rates resulting from bare ZnO at different concentrations, while panel (b) shows the degradation

This item was downloaded from IRIS Università di Bologna (<https://cris.unibo.it/>)

When citing, please refer to the published version.

rates obtained using ZnO doped with 1% of Ce synthesized from chloride salt. These supplemental tests showed an increase in the photochemical degradation rate at photocatalyst concentrations between 1500 mgL⁻¹ to 2000 mgL⁻¹, with a relative “optimum” result achieved at 1700 mgL⁻¹. At higher concentrations, the degradation rate decreases. Possible reasons for such a slowdown of phenol photodegradation rate are a detrimental effect of the photocatalyst due to back reactions (Minero and Vione, 2006) as well as adsorption of phenol on the catalytic material and/or saturation phenomena. Similar results occurred also with Er- and Yb-doped photocatalysts.

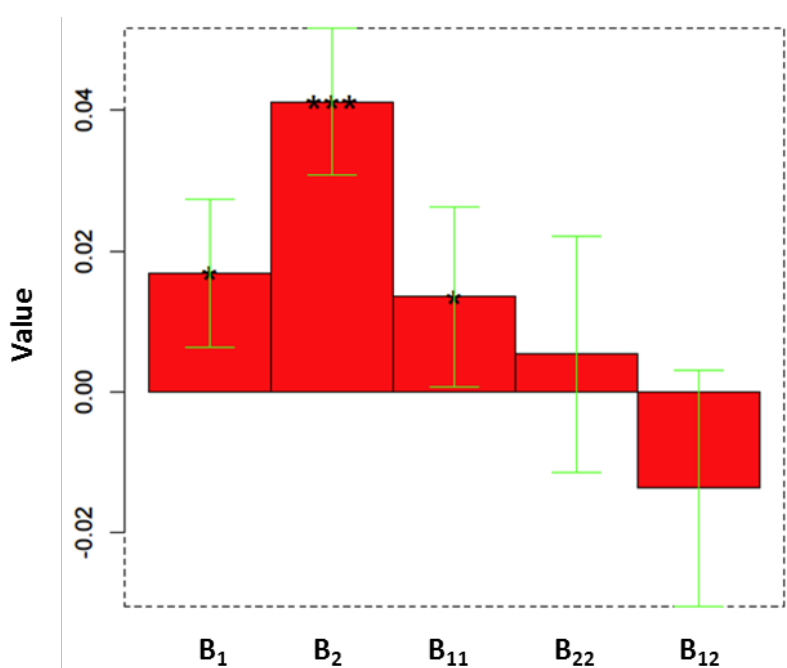


Figure 2. Estimation of the coefficients of the dopant (i.e., rare earth element) concentration in the photocatalyst (X_1) and of the concentration of the photocatalytic system employed in the degradation process (X_2). B_1 is the coefficient of the linear effect of X_1 , B_2 is the coefficient of the linear effect of X_2 , B_{11} is the coefficient of the quadratic effect of X_1 , B_{22} is the coefficient of the quadratic effect of X_2 , B_{12} is the coefficient of the interaction effect between X_1 and X_2 . Significance of coefficients – *: $p < 0.05$; **: $p < 0.01$; ***: $p < 0.001$).

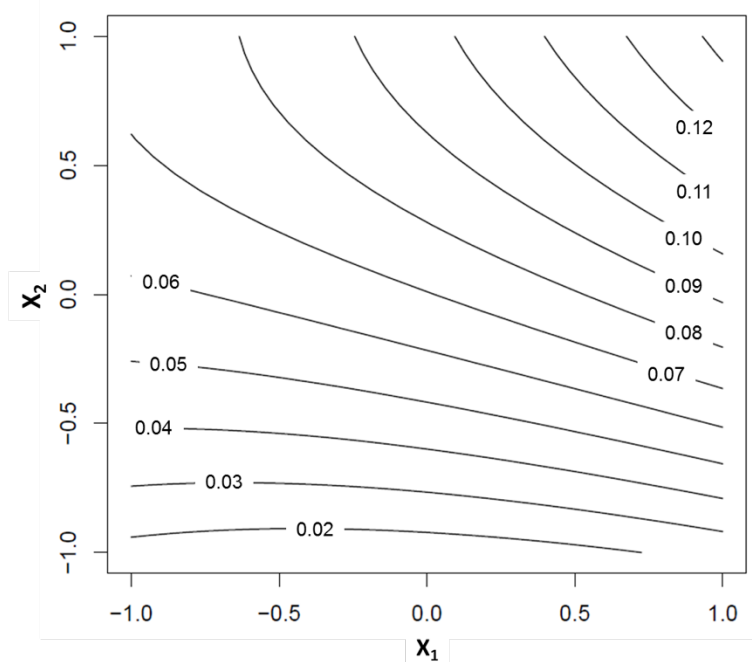


Figure 3. Response surface contour plot. X-axis and Y-axis show the investigated levels of rare earth element concentration (X_1) and photocatalyst concentration (X_2) in the experimental design.

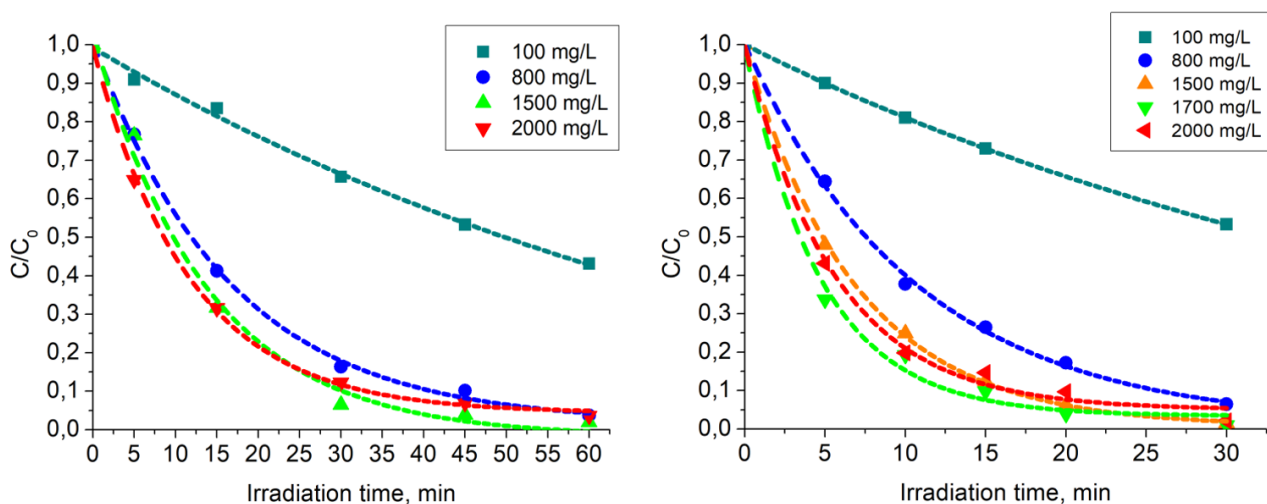


Figure 4. Reaction rate constant of phenol photodegradation at investigated concentrations of bare ZnO (on the left), and ZnO doped with 1% of cerium, synthesized from chloride salts CeZn1-Cl (on the right). C/C_0 indicates the ratio between the phenol concentration measured at a specific degradation time (C) and the initial concentration (C_0).

Table 3. Reaction rate constant (k , min^{-1}) of phenol degradation obtained in the presence of different photocatalysts as a function of photocatalyst concentration. The samples are labelled as XZp-S where X = dopant element (i.e., REE); Z = Zinc oxide; p = percentage of dopant in the photocatalysts (i.e., 0%, 0.5%, 1%); S = type of salt used for as dopant precursor (i.e., Cl or NO_3).

| k , min^{-1} | Photocatalyst concentration, mgL^{-1} | | | | |
|-------------------------|------------------------------------------------|-------|-------|-------|-------|
| Photocatalyst | 100 | 800 | 1500 | 1700 | 2000 |
| ZnO | 0.014 | 0.055 | 0.078 | | 0.059 |
| CeZn0.5-Cl | 0.020 | 0.077 | 0.085 | | |
| CeZn1-Cl | 0.021 | 0.088 | 0.139 | 0.152 | 0.128 |
| CeZn0.5- NO_3 | 0.012 | 0.074 | 0.109 | | |
| CeZn1- NO_3 | 0.014 | 0.074 | 0.114 | 0.167 | |
| ErZn0.5-Cl | 0.011 | 0.061 | | | 0.091 |
| ErZn1-Cl | 0.013 | 0.062 | | 0.127 | 0.100 |
| ErZn0.5- NO_3 | 0.012 | 0.048 | | | 0.081 |
| ErZn1- NO_3 | 0.014 | 0.062 | | 0.124 | 0.111 |
| YbZn0.5-Cl | 0.013 | 0.061 | | | 0.086 |
| YbZn1-Cl | 0.012 | 0.060 | | 0.107 | 0.084 |
| YbZn0.5- NO_3 | 0.011 | 0.062 | | | 0.109 |
| YbZn1- NO_3 | 0.012 | 0.066 | | 0.114 | 0.109 |

3.2 LCA for the photocatalytic process

Figure 5 shows LCIA results for the production of 1.7 g of CeZn1-Cl. The greatest energy requirement (i.e., about 98% of total CED) is associated with the electricity consumed during the sample treatment at 175°C overnight, followed by the energy required for the synthesis of ZnO from zinc nitrate and sodium hydroxide. Conversely, the synthesis of the dopant is marginal. Similar process contribution results were also achieved for Er- and Yb-doped photocatalytic systems with a relatively small deviation due to the production route of dopant precursors.

The effect of the photocatalyst concentration on the energy requirement is explored in Figure 6. CED results are computed as a function of CeZn1-Cl concentrations in the range 100-2000 mgL^{-1} . The complete degradation of 60 mgL^{-1} of phenol in 5 ml of solution was selected as the functional unit for comparison. At catalyst concentration of 100 mgL^{-1} , the complete photodegradation of phenol requires relatively longer irradiation time and it results in the largest amount of energy inputs. The system demands for the lowest energy inputs when the photocatalyst concentration is set at 800 mgL^{-1} . At higher concentrations, CED progressively increases but it remains lower than the energy inputs required at 100 mgL^{-1} . Absolute CED associated with electricity consumption is almost constant from 1500 to 2000 mgL^{-1} , suggesting that the

This item was downloaded from IRIS Università di Bologna (<https://cris.unibo.it/>)

When citing, please refer to the published version.

lowest energy requirement ensues at photocatalyst concentration $\geq 1500 \text{ mgL}^{-1}$. On the other hand, the synthesis of the photocatalyst at intermediate to high concentrations (i.e., 800-2000 mgL^{-1}) requires higher CED and results in up to about 75% of the total energy required.

Table 4 summarises LCA findings for the CED method providing the basis for comparing the kinetics outcomes in terms of energy requirements for phenol photodegradation. A heat map introduces a colour gradient that marks the results from red (the worst score) to green (the best score). Even if a combination of the fastest degradation rate with the lowest energy inputs is not achieved, the most promising outcome matches with Ce-doped (1%) ZnO and set the basis for the “best” working conditions.

In particular, the highest degradation rate was achieved with CeZn1- NO_3 at a concentration of 1700 mgL^{-1} , i.e. when employing the highest quantity of photocatalyst and dopant. The (relative) optimal working conditions could be achieved by reducing the photocatalyst concentration from 1700 mgL^{-1} to 1500 mgL^{-1} . This reduction would result in only 9% decrease of the degradation rate. In contrast, the lowest energy requirement seems to occur for CeZn1-Cl at 800 mgL^{-1} . Setting the concentration of CeZn1-Cl at 1500 mgL^{-1} and 1700 mgL^{-1} determines respectively an increase of 11% and 18% in CED results. From this, the optimal conditions for the degradation of phenol in water are reasonably obtained when CeZn1-Cl is in the range 800-1500 mgL^{-1} .

The relative global warming contribution results are summarized in Table 5 and displayed in Figure 6 and Figures S6-S7 in the SI. The synthesis process results in the release of 1.8 kg CO_2 eq to produce 1.7 g of CeZn1-Cl (Figure S6). Setting the best operational conditions identified above, the photodegradation of phenol would determine the release of 11.5-13.2 gCO_2 eq.

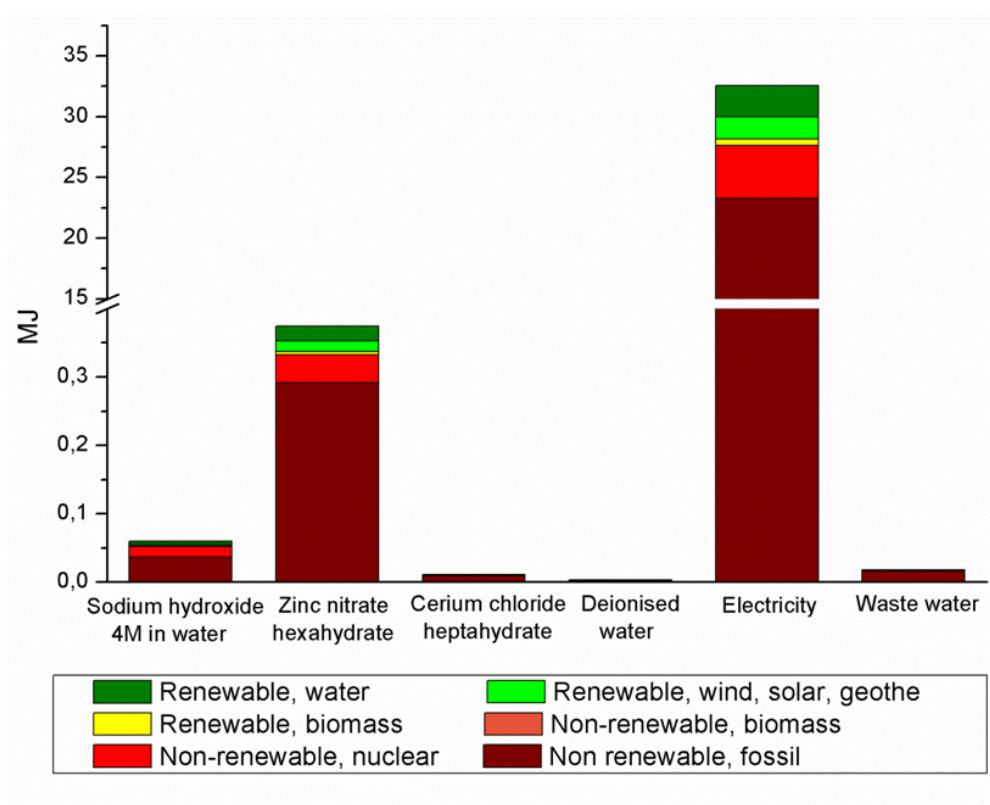


Figure 5. Cumulative Energy Demand (CED) and process contribution associated with the synthesis of 1.7 g of Ce-doped ZnO photocatalyst (i.e., CeZn1-Cl).

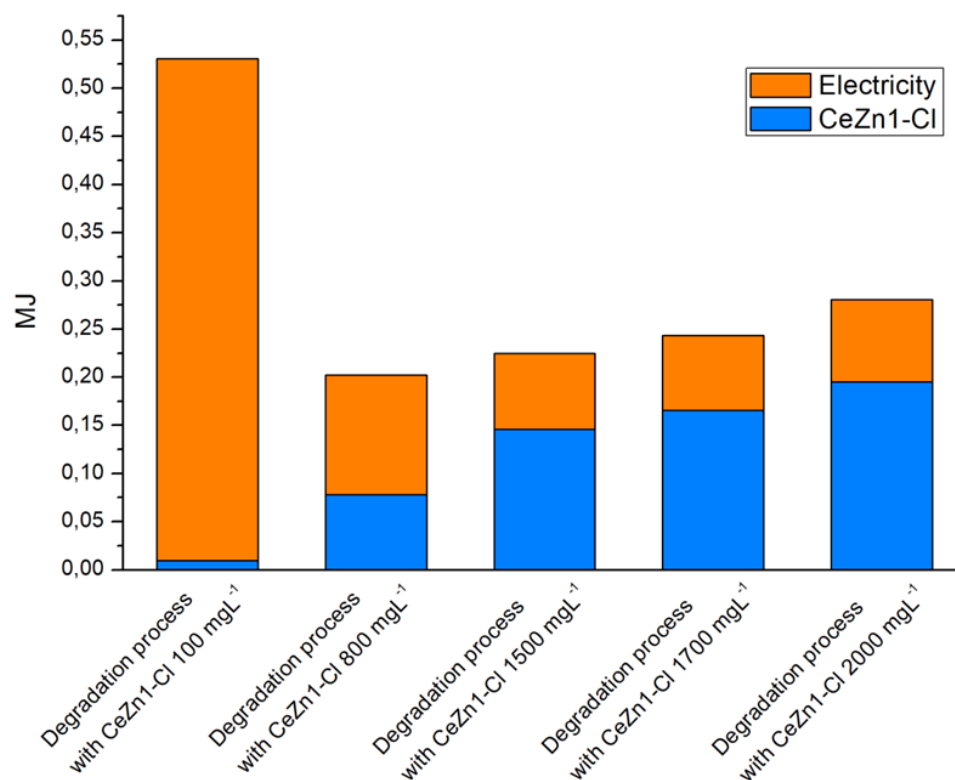


Figure 6. Cumulative Energy Demand (MJ) for the degradation process as a function of the photocatalyst concentration.

Table 4. Life cycle impact assessment results for Cumulative Energy Demand (CED) associated with the samples investigated. The heat map introduces a colour gradient that differentiates the results from red (the worst score) to green (the best score). The samples are labelled as YZp-S where Y = dopant element (i.e., REE); Z = Zinc oxide; p = percentage of dopant in the photocatalysts (i.e, 0%, 0.5%, 1%); S = type of salt used for as dopant precursor (i.e., Cl or NO₃).

| Photocatalyst | CED (MJ) | | | | |
|-------------------------|-----------------------|-----------------------|------------------------|------------------------|------------------------|
| | 100 mgL ⁻¹ | 800 mgL ⁻¹ | 1500 mgL ⁻¹ | 1700 mgL ⁻¹ | 2000 mgL ⁻¹ |
| ZnO | 792 | 280 | 292 | | 388 |
| CeZn0.5- Cl | 557 | 222 | 278 | | |
| CeZn1- Cl | 531 | 202 | 225 | 238 | 280 |
| CeZn0.5-NO ₃ | 922 | 227 | 249 | | |
| CeZn1-NO ₃ | 792 | 226 | 242 | 231 | |
| ErZn0.5-Cl | 1010 | 259 | | | 318 |
| ErZn1-Cl | 852 | 254 | | 251 | 303 |
| EZ0.5-H NO ₃ | 922 | 307 | | | 333 |
| ErZn1-NO ₃ | 792 | 254 | | 253 | 292 |
| YbZn0.5-Cl | 852 | 259 | | | 326 |
| YbZn1-Cl | 922 | 260 | | 267 | 324 |
| YbZn0.5-NO ₃ | 1010 | 256 | | | 299 |
| YbZn1-NO ₃ | 922 | 243 | | 261 | 294 |

Table 5. Life cycle impact assessment results for IPCC 2013 GWP 100y. The heat map introduces a colour gradient that differentiates the results from red (the worst score) to green (the best score). The samples are labelled as YZp-S where Y = dopant element (i.e., REE); Z = Zinc oxide; p = percentage of dopant in the photocatalysts (i.e, 0%, 0.5%, 1%); S = type of salt used for as dopant precursor (i.e., Cl or NO₃).

| Photocatalyst | IPCC 2013 GWP 100y (g CO ₂ eq) | | | | |
|-------------------------|-------------------------------------------|-----------------------|------------------------|------------------------|------------------------|
| | 100 mgL ⁻¹ | 800 mgL ⁻¹ | 1500 mgL ⁻¹ | 1700 mgL ⁻¹ | 2000 mgL ⁻¹ |
| ZnO | 45.0 | 15.9 | 16.7 | | 22.1 |
| CeZn0.5- Cl | 31.7 | 12.6 | 15.8 | | |
| CeZn1-Cl | 30.2 | 11.5 | 12.8 | 13.9 | 16.0 |
| CeZn0.5-NO ₃ | 52.4 | 12.9 | 14.2 | | |
| CeZn1-NO ₃ | 45.0 | 12.9 | 13.8 | 13.2 | |
| ErZn0.5-Cl | 57.1 | 14.7 | | | 18.2 |
| ErZn1-Cl | 48.4 | 14.5 | | 14.3 | 17.3 |
| ErZn0.5-NO ₃ | 52.4 | 17.5 | | | 19.0 |
| ErZn1-NO ₃ | 45.0 | 14.5 | | 14.4 | 16.7 |
| YbZn0.5-Cl | 48.4 | 14.7 | | | 18.6 |
| YbZn1-Cl | 52.4 | 14.8 | | 15.2 | 18.5 |
| YbZn0.5-NO ₃ | 57.1 | 14.6 | | | 17.0 |
| YbZn1-NO ₃ | 52.4 | 13.8 | | 14.9 | 16.8 |

This item was downloaded from IRIS Università di Bologna (<https://cris.unibo.it/>)

When citing, please refer to the published version.

3.3 Implications for theory, and practice

As demonstrated in this work, the overall degradation rate of ZnO photocatalytic systems is increased if REEs are used as dopants. A possible explanation can be attributed to the existence of intra-band gap states that would allow the absorption of visible photons. The number of electrons in the *f* orbitals seems to play a primary role in the degradation activity as, generally, at higher atomic number *Z* of doping REEs correspond higher *k* constants. (Sarro et al., 2017)

For cerium oxide, however, the greater degradation efficiency shown can be likely related to its electronic structure, with possible transition of electrons between the valence band (i.e., oxygen 2p orbitals) and 4f orbitals that are partially filled in the case of Ce³⁺ or empty in Ce⁴⁺ (Calza et al., 2017). Although the structure of ZnO is preserved when doping it with cerium oxide, some interactions at the interfaces of the two oxides may occur. Compared to other dopants, CeO₂ and ZnO form a biphasic system that may result in enhancing the photochemical degradation of phenol, with the Ce oxide promoting some electron transfer from the discrete 4f levels to the bulk zinc oxide (Cerrato et al., 2018). Regarding the charge carrier separation, Er showed an improved photocurrent, Yb a better accumulation of photoelectrons, while faster electron transfer resulted for Ce-doped ZnO. Direct photolysis and adsorption of phenol on the photocatalysts surface in the dark scarcely contributed to phenol attenuation (Sordello et al., 2019).

Advanced oxidation processes like the heterogeneous photocatalytic method investigated in this study are promising ways to achieve high standards of wastewater purification and environmental protection. Of more interest here, the hydrothermal production route discussed in this study is relatively simple and enables to synthesize controlled nanostructures at low temperatures. On field, heterogeneous catalytic systems are capable to use solar light for the abatement of organic pollutants, making this technique cheaper, portable and more versatile than traditional photocatalysts. Furthermore, the possibility of exploiting solar light to promote photodegradation phenomena will enable to count on a potentially renewable energy source with consequential benefits in climate mitigation effects.

Notwithstanding this study provides novel insights about the overall degradation process related to ZnO photocatalytic systems, we believe that more research is needed to further understanding the underlying electron transfer phenomena as well as further assessments (e.g., life cycle costing) to scale this technique up to real systems. Although an economic assessment is out of the scope of our study, the main economic advantages of REEs-doped ZnO photocatalysts can be pointed out. First, ZnO is cheaper than other photocatalysts on market (e.g., TiO₂). Second, the precursors considered in the synthesis are commercially available and the relatively low concentration of dopants in the catalytic system are not expected to affect significantly the overall cost. Lastly, material requirements and costs can benefit from a regeneration of the photocatalyst. In the literature, the use of polymers nanofibers is discussed as a possible support for catalytic

This item was downloaded from IRIS Università di Bologna (<https://cris.unibo.it/>)

When citing, please refer to the published version.

applications in virtue of their high surface area to volume ratio and, consequently, of the loading capacity of the substrate. Among others, thanks to its features of biocompatibility and cost efficiency, poly(styrene-co-maleic anhydride) provides promising expectations toward the development of full scale supported treatment systems for the removal of pollutants in wastewater (Sarro et al., 2017).

4. Conclusions

Guaranteeing water quality and water access for all is one of the main objectives of a sustainable development. Diversifying and augmenting water sources includes also the potential treatment of polluted water streams and wastewaters upon fulfilling of quality and safe standard requirements. Among others, heterogeneous catalysis, with REEs-doped ZnO photocatalytic systems being an example of particular interest, have the potential for achieving an efficient removal of pollutants at relatively low cost. A full implementation of REEs-doped ZnO, however, comes also through a systematic evaluation of operating conditions to set the basis for achieving the greatest degradation efficiency at the preferable environmental performance.

The results of this study pointed out that even if the highest degradation efficiency is obtained with 1700 mgL⁻¹ of ZnO doped with 1% of Ce from nitrate precursor, setting the photocatalyst concentration at 800 mgL⁻¹ may be preferable to reduce the environmental impacts, and likely the economic costs, associated with the input of electrical energy and the synthesis procedure. To this aim, however, the chance of exploiting the solar light to promote photocatalysis and the possibility to hold the catalyst on supports that may facilitate its recovery for regeneration are of great interest for a full implementation of ZnO-based advanced oxidation processes at lower economic and environmental cost.

Data used to model the system were obtained at the laboratory scale and can only offer a partial view of the real behavior of these materials. This is a main limitation to the feasible scaling up of laboratory processes to real systems. Therefore, perspectives for future works include the assessment of photodegradation in real wastewater matrixes. To this aim, a combination of DoE and LCA is highly recommended to assess the environmental performance of the entire domain of the system under scrutiny.

Acknowledgments

We acknowledge support from a Marie Curie International Research Staff Exchange Scheme Fellowship (MAT4TREAT, proposal no. 645551) within the Horizon 2020 European Community Framework Programme.

Supporting Information. In the supporting information file, both the significance of coefficients for all the REEs-doped ZnO from chloride and nitrate precursors, and the response surface contour plot for all the

This item was downloaded from IRIS Università di Bologna (<https://cris.unibo.it/>)

When citing, please refer to the published version.

photocatalysts were reported. Also the degradation curves obtained for the degradation of the phenol were showed; the curves were grouped per type of element used as dopant. The LCIA results, using the Global Warming Potential IPCC 2013 GWP 100y method, of the synthesis of CeZn1-Cl were also reported, as well as the comparison of the LCIA results for the degradation process using CeZn1-Cl at different concentration, results obtained using the IPCC 2013 GWP 100y method.

References

- Althaus, H.-J., Chudacoff, M., Hirschier, R., Osses, M., Primas, A., 2007. Life Cycle Inventories of Chemicals. Final report ecoinvent data v2.0 No. 8. Swiss Centre for Life Cycle Inventories, Dübendorf, CH.
- Asadollahi, M., Bastani, D., Musavi, S.A., 2017. Enhancement of surface properties and performance of reverse osmosis membranes after surface modification: A review. *Desalination*. 420, 330-383.
- August, M., 1965. Process for preparing pulverulent hydrates of zinc nitrate. Patent US3206281A.
- Binnemans, K., Jones, P. T., Blanpain, B., Gerven, T. V., Yang, Y., Walton, A., Buchert, M., 2013. Recycling of rare earths: a critical review. *J. Clean. Prod.* 51, 1-22.
- Blanchard, A. A., Phelan, J. W., Davis, A. R., 1936. *Synthetic Inorganic Chemistry*. Fifth edition. New York, pp. 286-287.
- Bolisetty, S., Peydayesh, M., Mezzenga, R., 2019. Sustainable technologies for water purification from heavy metals: review and analysis. *Chem. Soc. Rev.* 48, 463-487
- Calza, P., Gionco, C., Giletta, M., Kalaboka, M., Sakkas, V. A., Albanis, T., Paganini, M. C., 2017. Assessment of the Abatement of Acelsulfame K Using Cerium Doped ZnO as Photocatalyst. *J. Hazard. Mater.* 323, 471-477.
- Capocelli, M., Prisciandaro, M., Piemonte, V., Barba, D., 2019. A technical-economical approach to promote the water treatment & reuse processes. *J. Clean. Prod.* 207, 85-96.
- Cerrato, E., Gionco, C., Paganini, M. C., Giamello, E., Albanese, E., Pacchioni, G., 2018. Origin of visible light photoactivity of the CeO₂/ZnO heterojunction. *Appl. Energy Mater.* 1, 8, 4247-4260.
- Chiou, C.-H., Juang, R.-S., 2007. Photocatalytic degradation of phenol in aqueous solutions by Pr-doped TiO₂ nanoparticles. *J. Hazard. Mater.* 149, 1-7. <https://doi.org/10.1016/j.jhazmat.2007.03.035>
- Ciacci, L., Vassura, I., Cao, Z., Liu, G., Passarini, F., 2019. Recovering the “new twin”: Analysis of secondary neodymium sources and recycling potentials in Europe. *Resour. Conserv. Recycl.* 142, 143-152.
- De Faria A. B. B., Spérandio, M., Ahmadi, A., Tiruta-Barna, L., 2015. Evaluation of new alternatives in wastewater treatment plants based on dynamic modelling and life cycle assessment (DM-LCA). *Water Research*. 84, 99-111.
- Díaz-Madronero, M., Pérez-Sánchez, M., Satorre-Aznar, J. R., Mula, J., López-Jiménez, P. A., 2018. Analysis of a wastewater treatment plant using fuzzy goal programming as a management tool: A case study. *J. Clean. Prod.* 180, 20-33.
- Dirk van der Kooij, D., van der Wielen. P. W. J. J., 2014. *Microbial Growth in Drinking-Water Supplies: Problems, Causes, Control and Research Needs*. IWA Publishing, London U.K.

This item was downloaded from IRIS Università di Bologna (<https://cris.unibo.it/>)

When citing, please refer to the published version.

- Friedrich, E., 2002. Life-cycle assessment as an environmental management tool in the production of potable water. *Water Sci. Technol.* 46, 29–36.
- Frischknecht, R., Editors, N. J., Althaus, H., Bauer, C., Doka, G., Dones, R., Hirschier, R., Hellweg, S., Köllner, T., Loerincik, Y., Margni, M., Nemecek, T., 2007. Implementation of Life Cycle Impact Assessment Methods.
- Garrone, P., Grilli, L., Groppi, A., Marzano, R., 2018. Barriers and drivers in the adoption of advanced wastewater treatment technologies: a comparative analysis of Italian utilities. *J. Clean. Prod.* 171, S69–S78.
- Gjorgiev, B., Sansavini, G., 2017. Water-energy nexus: Impact on electrical energy conversion and mitigation by smart water resources management. *Energy Conversion and Management.* 148, 1114–1126.
- Gruppo di Chemiometria, 2019. Chemometric Agile Tool (CAT). Available at: <http://www.gruppochemiometria.it/index.php/software/19-download-the-r-based-chemometric-software>
- Gupta, C. K., Krishnamurthy, N., 2005. Extractive metallurgy of rare earth. CRC press LLC.
- Heijungs, R. and Koning, A., 2004. Improvement of LCA characterization factors and LCA practice for metals. TNO Report- E 2004/347, August 2004, International Council on Minings and Metals .
- Hellman, P. L., Duncan, R. K., 2014. Evaluation of Rare Earth Element Deposits. *Appl. Earth Sci.* 123 (2), 107–117. <https://doi.org/10.1179/1743275814Y.0000000054>.
- Homem, V., Santos, L., 2011. Degradation and removal methods of antibiotics from aqueous matrices – A review. *Journal of Environmental Management.* 92, 2304–2347.
- Houghton J. T., Ding, Y., Griggs, D. J., Noguer, M., van der Linden, P. J., Dai, X., Maskell, K., Johnson, C., 2001. Climate Change 2001: The Scientific Basis. Contribution of Working Group I to the Third Assessment Report of the Intergovernmental Panel on Climate Change; Cambridge University Press, Cambridge, United Kingdom and New York, NY, USA. <https://doi.org/10.1256/004316502320517344>.
- ISO – International Organization for Standardization, 2006a. 14040 – Environmental management, Life cycle assessment, Principles and framework. Available at: <https://www.iso.org/standard/37456.html> (accessed on October 2019)
- ISO – International Organization for Standardization, 2006b. 14044 – Environmental management, Life cycle assessment, Requirements and guidelines. Available at: <https://www.iso.org/standard/37456.html> (accessed on October 2019)
- Koltun, P., Tharumarajah, A., 2014. Life Cycle Impact of Rare Earth Elements. *ISRN Metall.* 2014, 10 pages. <https://doi.org/10.1155/2014/907536>.
- Krozer, Y., Hophmayer-Tokich, S., van Meerendonk, H., Tijssma, S., Eric Vos, E., 2010. Innovations in the water chain – experiences in The Netherlands. *J. Clean. Prod.* 18, 439–446.
- Kumar, A., Pandey, G., 2017. A Review on the Factors Affecting the Photocatalytic Degradation of Hazardous Materials. *Mater. Sci. Eng. Int. J.* 1 (3), 1–10. <https://doi.org/10.15406/mseij.2017.01.00018>.
- Larsen, M. A. D., Drews, M., 2019. Water use in electricity generation for water-energy nexus analyses: The European case. *Sci. Total Environ.* 651, 2044–2058.
- Lee, K. M.; Lai, C. W.; Ngai, K. S.; Juan, J. C.; Recent developments of zinc oxide based photocatalyst in water treatment technology: A review. *Water Research.* 2015, 88, 428–448. <http://dx.doi.org/10.1016/j.watres.2015.09.045>.

This item was downloaded from IRIS Università di Bologna (<https://cris.unibo.it/>)

When citing, please refer to the published version.

- Liu, J., Mooney, H., Hull, V., Davis, S.J., Gaskell, J., Hertel, T., Lubchenco, J., Seto, K. C., Gleick, P., Kremen, C., Li, S., 2015. Systems integration for global sustainability. *Science*. 347 (6225), 1258832.
- Márquez, J. A. R., Herrera, C. M., Fuentes, M. L., Rosas, L. M., 2012. Effect of Three Operating Variables on Degradation of Methylene Blue by ZnO Electrodeposited: Response Surface Methodology. *Int. J. Electrochem. Sci.* 7 (11), 11043–11051.
- Mehta, D., Mazumdar, S., Singh, S.K., 2015. Magnetic adsorbents for the treatment of water/wastewater—A review. *Jorunal of Water Process Engineering*. 7, 244–265.
- Mekonnen, M. M., Gerbens-Leenes, P. W., Hoekstra, A. Y., 2015. The consumptive water footprint of electricity and heat: a global assessment. *Environ. Sci. Water Res. Technol.* 1, (3), 285–297. DOI:10.1039/c5ew00026b.
- Meneses, M., Pasqualino, J. C., Castells, F., 2010. Environmental assessment of urban wastewater reuse: Treatment alternatives and applications. *Chemosphere*. 81, 266–272.
- Minero, C., Vione, D., 2006. A Quantitative Evaluation of the Photocatalytic Performance of TiO₂ slurries. *Appl. Catal. B Environ.* 67, 257–269. <https://doi.org/10.1016/j.apcatb.2006.05.011>.
- Mo, W., Wang, R., Zimmerman, J. B., 2014. Energy–Water Nexus Analysis of Enhanced Water Supply Scenarios: A Regional Comparison of Tampa Bay, Florida, and San Diego, California. *Environ. Sci. Technol.* 48, 5883–5891.
- Morera, S., Corominas, L. I., Poch, M., Aldaya, M., Comas, J., 2016. Water footprint assessment in wastewater treatment plants. *J. Clean. Prod.* 112, 4741–4748.
- Navarro, J., Zhao, F., 2014. Life-Cycle Assessment of the Production of Rare-Earth Elements for Energy Applications: A Review. *Front. Energy Res.* 2, 45. <https://doi.org/10.3389/fenrg.2014.00045>
- Nuss, P., Eckelman, M., 2014. J. Life Cycle Assessment of Metals: A Scientific Synthesis. *PLoS ONE*. 9(7): e101298. <https://doi.org/10.1371/journal.pone.0101298>.
- Ortiz, F. R., Rose, J., Speight, V., von Gunten, U., Schnoor, J., 2016. How do you like your tap water? *Science*. 351 (6276), 912–914.
- Pasqualino, J. C., Meneses, M., Castells, F., 2011. Life cycle assessment of urban wastewater reclamation and reuse alternatives. *J. Ind. Ecol.* 15, 49–63.
- Peiró, L. T., Méndez, G. V., 2013. Material and Energy Requirement for Rare Earth Production. *JOM*. 65 (10), 1327–1340. <https://doi.org/10.1007/s11837-013-0719-8>.
- Pitts, F., 1979. Preparation of rare earth nitrates. Patent US4231997A.
- Ramírez, Y., Kraslawski, A., Cisternas, L. A., 2019. Decision-support framework for the environmental assessment of water treatment systems. *J. Clean. Prod.* 225, 599–609.
- Reza, K. M., Kurny, A., Gulshan, F., 2017. Parameters Affecting the Photocatalytic Degradation of Dyes Using TiO₂: A Review. *Appl. Water Sci.* 7 (4), 1569–1578. <https://doi.org/10.1007/s13201-015-0367-y>.
- Rodriguez-Garcia, G., Molinos-Senante, M., Hospido, A., Hernandez-Sancho, F., Moreira, M., Feijoo, G., 2011. Environmental and economic profile of six typologies of wastewater treatment plants. *Water Res.* 45, 5997–6010.
- Rumble, J. R., 2018. CRC Handbook of Chemistry and Physics, 99th Edition.
- Sabeen, A. H., Noor, Z. Z., Ngadi, N., Almuraisy, S., Raheem, A. B., 2018. Quantification of environmental impacts of domestic wastewater treatment using life cycle assessment: A review. *J. Clean. Prod.* 190, 221–233.

This item was downloaded from IRIS Università di Bologna (<https://cris.unibo.it/>)

When citing, please refer to the published version.

- Sarro, M., Gule, N. P., Laurenti, E., Gamberini, R., Paganini, M. C., Mallon, P. E., Calza, P., 2017. ZnO-based materials and enzymes hybrid systems as highly efficient catalysts for recalcitrant pollutants abatement. *Chem. Eng. J.* 334, 2530-2538.
- Schulze, R., Weidema, B. P., Schebek, L., Buchert, M., 2018. Recycling and its effects on joint production systems and the environment – the case of rare earth magnet recycling – Part I — Production model. *Resources, Conservation and Recycling.* 134, 336-346.
- Sebastian, J., Seifert, H.-J., 1998. Ternary chlorides in the systems $ACl/YbCl_3$ ($A=Cs,Rb,K$); *Thermochimica Acta.* 318, 29-37 [https://doi.org/10.1016/S0040-6031\(98\)00326-8](https://doi.org/10.1016/S0040-6031(98)00326-8).
- Sordello, F.; Berruti, I.; Gionco, C.; Paganini, M. C.; Calza, P.; Minero, C. Photocatalytic Performances of Rare Earth Element-Doped Zinc Oxide toward Pollutant Abatement in Water and Wastewater. *Appl. Catal. B Environ.* 2019, 245, 159–166.
- Sovacool, B.K.; Sovacool, K.E. Identifying future electricity-water tradeoffs in the United States. *Energy policy* 2009, 37, 2763-2773.
- Specher, B., Xiao, Y., Walton, A., Speight, J., Harris, R., Kleijn, R., Visser, G., Kramer G.J., 2014. Life cycle inventory of the production of rare earths and the subsequent production of NdFeB rare earth permanent magnets. *Environ. Sci. Technol.* 48, 3951-3958.
- Stokes, J., Horvath, A., 2006. Life cycle energy assessment of alternative water supply systems. *Int. J. Life Cycle Assess.* 11, 335–343.
- Sustainable development goals knowledge platform. <https://sustainabledevelopment.un.org/> (accessed on March 2019)
- Warsinger, D. M., Chakraborty, S., Tow, E. W., Plumlee, M. H., Bellona, C., Loutatidou, S., Karimi, L., Mikelonis, A. M., Achilli, A., Ghassemi, A., Padhye, L. P., Snyder, S. A., Curcio, S., Vecitis, C. D., Arafat, H.A., Lienhard, J. H., 2018. A review of polymeric membranes and processes for potable water reuse. *Progress in Polymer Science.* 81, 209-237.
- World economic forum, 2018. <https://www.weforum.org/agenda/2018/09/this-is-how-we-can-fight-water-scarcity/> (accessed on March 2019)
- Yang, Y., Walton, A., Sheridan, R., Güth, K., Gauß, R., Gutfleisch, O., Buchert, M., Steenari, B. M., Gerven, T. V., Jones, P. T., Binnemans, K., 2016. REE Recovery from End-of-Life NdFeB Permanent Magnet Scrap: A Critical Review. *J. Sustain. Metall.* 3, 122–149.
- Zakotnik, M., Tudor, C. O., Peiró, L. T., Afiuny, P., Skomski, R., Hatch, G. P., 2016. Analysis of energy usage in Nd–Fe–B magnet to magnet recycling. *Environ. Technol. Innov.* 5, 117-126.

Combining the highest degradation efficiency with the lowest environmental impact in zinc oxide based photocatalytic systems

Mattia Costamagna¹, Luca Ciacci², Maria Cristina Paganini¹, Paola Calza¹, Fabrizio Passarini^{2,3}

¹Department of Chemistry, University of Turin, Via P. Giuria 7, 10125 Torino, Italy

²Department of Industrial Chemistry “Toso Montanari”, University of Bologna, Viale del Risorgimento 4,
40136 Bologna, Italy

³Interdepartmental Centre for Industrial Research “Renewable Resources, Environment, Sea and Energy”,
University of Bologna, Via D. Campana 71, 47922, Rimini

Supporting Information

This item was downloaded from IRIS Università di Bologna (<https://cris.unibo.it/>)

When citing, please refer to the published version.

Number of pages: 9
 Number of tables: 1
 Number of figures: 7

Table S1. Full experimental matrix for the FCD model. The samples are labelled as YZp-S where Y = dopant element (i.e., REE); Z = Zinc oxide; p = percentage of dopant in the photocatalysts (i.e, 0%, 0.5%, 1%); S = type of salt used for as dopant precursor (i.e., chloride or nitrates).

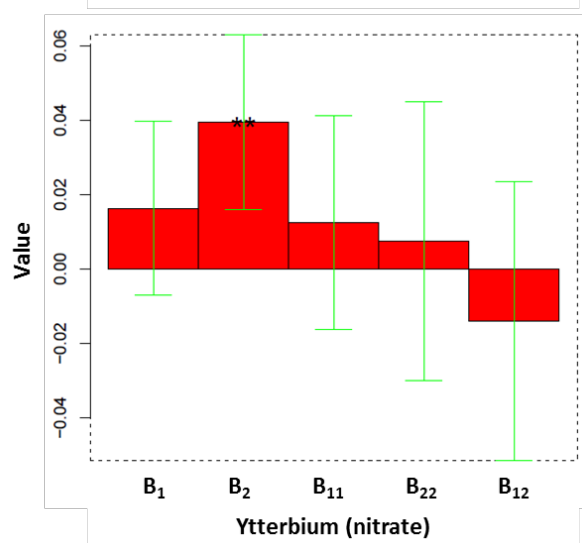
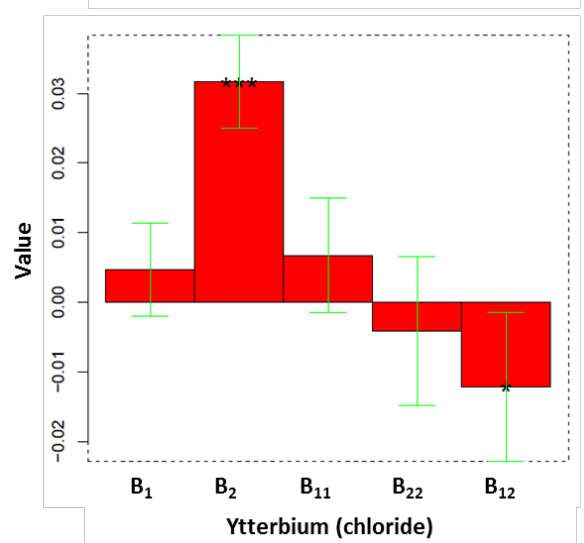
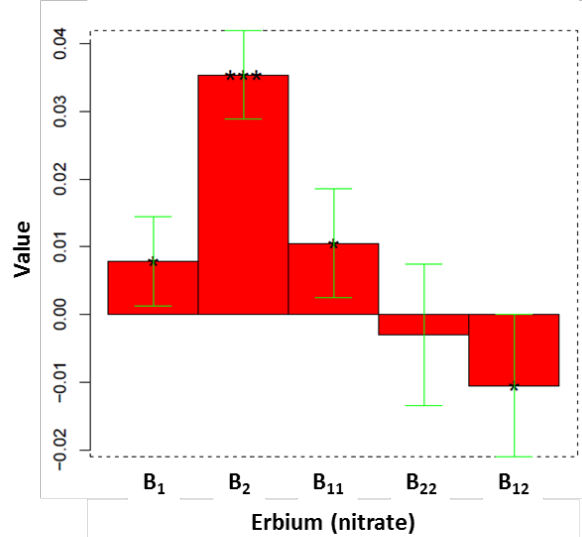
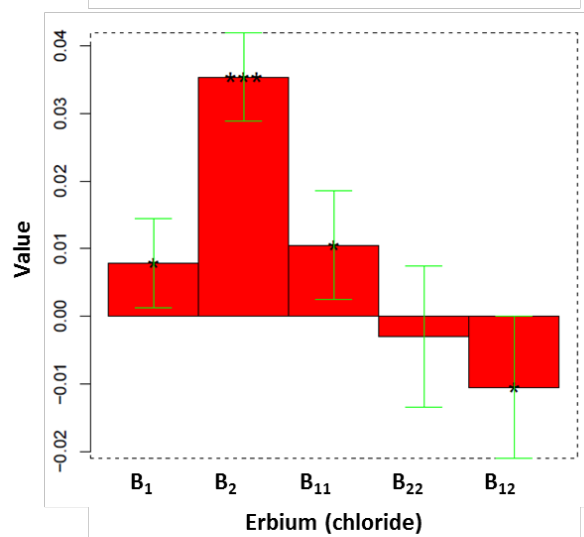
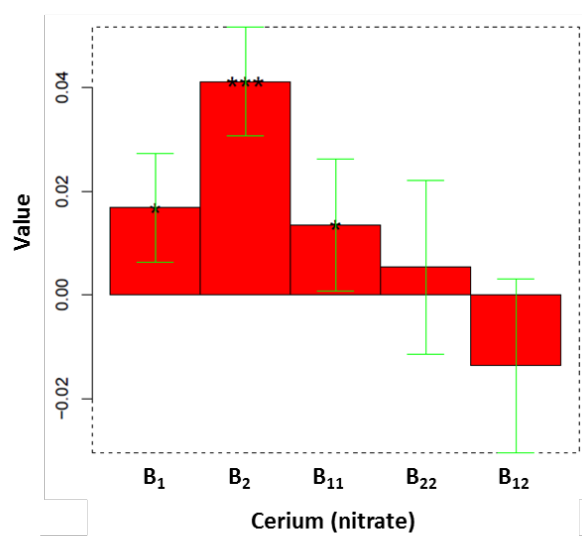
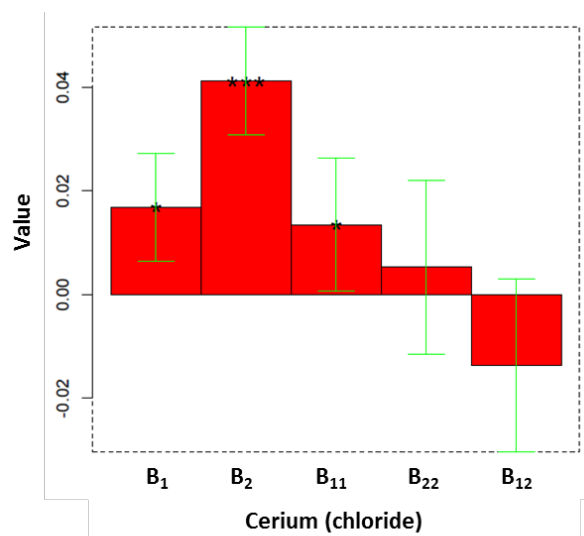
| ZnO doped with cerium | | | | | |
|------------------------------|--------|-------------------------|-------------------|--------|-------------------------|
| Chloride precursor | | | Nitride precursor | | |
| n. exp | [Ce]/% | [cat]/mgL ⁻¹ | n. exp | [Ce]/% | [cat]/mgL ⁻¹ |
| 1 | 0.5 | 800 | 1 | 0.5 | 800 |
| 2 | 1.0 | 1500 | 2 | 1.0 | 1500 |
| 3 | 1.0 | 800 | 3 | 1.0 | 800 |
| 4 | 0.5 | 100 | 4 | 0.5 | 100 |
| 5 | 0.0 | 800 | 5 | 0.0 | 800 |
| 6 | 0.0 | 100 | 6 | 0.0 | 100 |
| 7 | 1.0 | 100 | 7 | 1.0 | 100 |
| 8 | 0.0 | 1500 | 8 | 0.0 | 1500 |
| 9 | 0.5 | 1500 | 9 | 0.5 | 1500 |
| 10 | 0.5 | 800 | 10 | 0.5 | 800 |

| ZnO doped with erbium | | | | | |
|------------------------------|--------|--------------------------|-------------------|--------|--------------------------|
| Chloride precursor | | | Nitride precursor | | |
| n. exp | [Er]/% | [cat]/ mgL ⁻¹ | n. exp | [Er]/% | [cat]/ mgL ⁻¹ |
| 1 | 0.5 | 800 | 1 | 0.5 | 800 |
| 2 | 1.0 | 2000 | 2 | 1.0 | 2000 |
| 3 | 1.0 | 800 | 3 | 1.0 | 800 |
| 4 | 0.5 | 100 | 4 | 0.5 | 100 |
| 5 | 0.0 | 800 | 5 | 0.0 | 800 |
| 6 | 0.0 | 100 | 6 | 0.0 | 100 |
| 7 | 1.0 | 100 | 7 | 1.0 | 100 |
| 8 | 0.0 | 2000 | 8 | 0.0 | 2000 |
| 9 | 0.5 | 2000 | 9 | 0.5 | 2000 |
| 10 | 0.5 | 800 | 10 | 0.5 | 800 |

| ZnO doped with ytterbium | | | | | |
|---------------------------------|--------|--------------------------|-------------------|--------|--------------------------|
| Chloride precursor | | | Nitride precursor | | |
| n. exp | [Yb]/% | [cat]/ mgL ⁻¹ | n. exp | [Yb]/% | [cat]/ mgL ⁻¹ |
| 1 | 0.5 | 800 | 1 | 0.5 | 800 |
| 2 | 1.0 | 2000 | 2 | 1.0 | 2000 |
| 3 | 1.0 | 800 | 3 | 1.0 | 800 |
| 4 | 0.5 | 100 | 4 | 0.5 | 100 |
| 5 | 0.0 | 800 | 5 | 0.0 | 800 |
| 6 | 0.0 | 100 | 6 | 0.0 | 100 |
| 7 | 1.0 | 100 | 7 | 1.0 | 100 |
| 8 | 0.0 | 2000 | 8 | 0.0 | 2000 |
| 9 | 0.5 | 2000 | 9 | 0.5 | 2000 |
| 10 | 0.5 | 800 | 10 | 0.5 | 800 |

This item was downloaded from IRIS Università di Bologna (<https://cris.unibo.it/>)

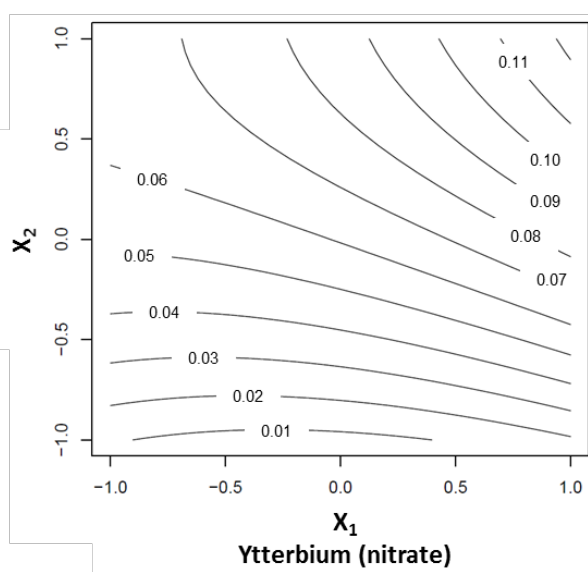
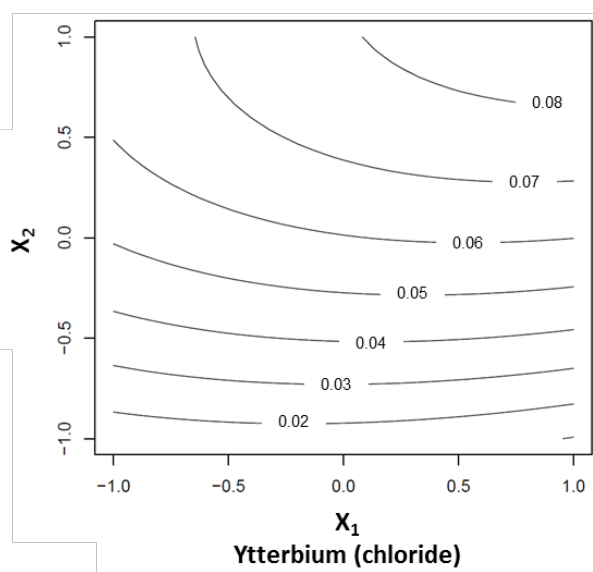
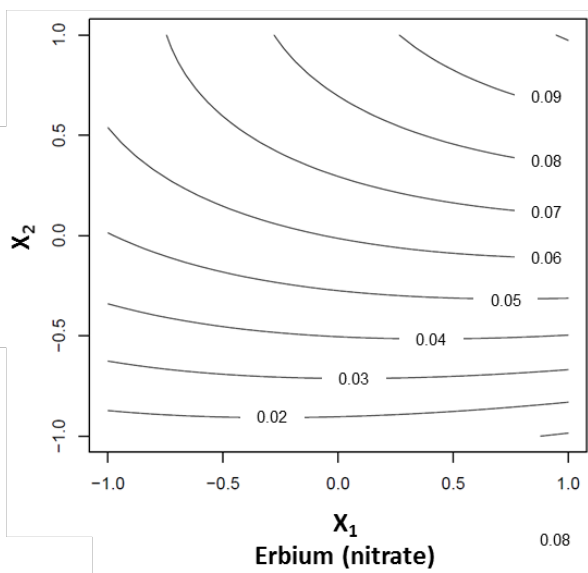
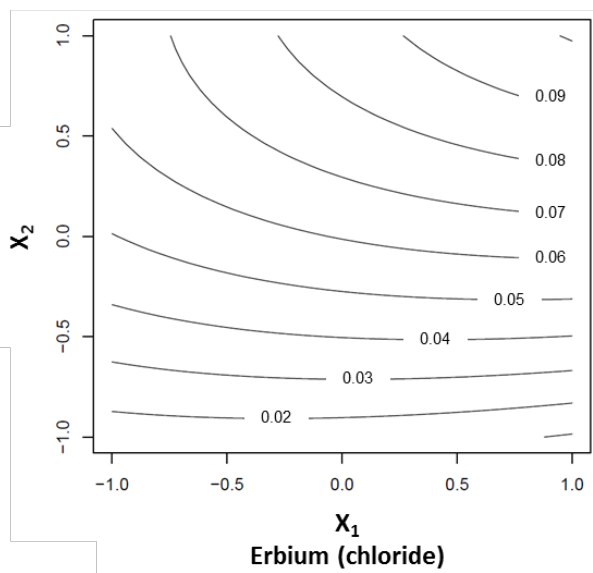
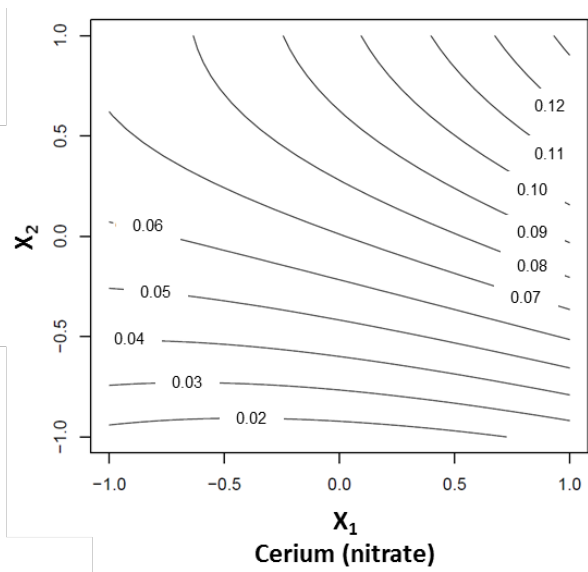
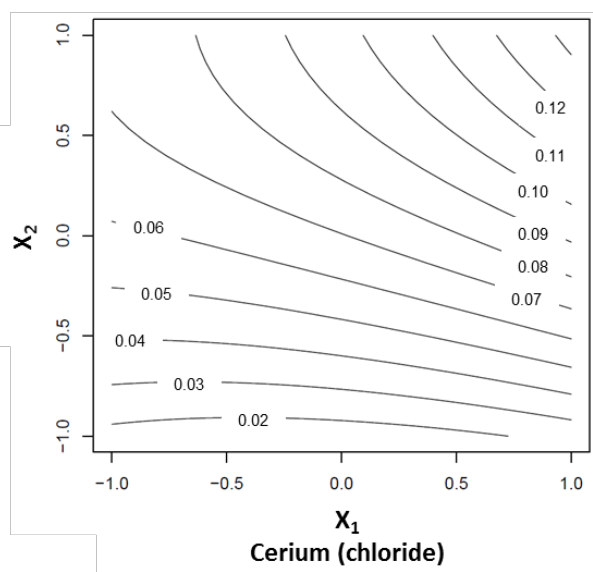
When citing, please refer to the published version.



This item was downloaded from IRIS Università di Bologna (<https://cris.unibo.it/>)

When citing, please refer to the published version.

Figure S1. Estimation of the coefficients of the dopant (i.e., rare earth element) concentration in the photocatalyst from chloride and nitrate precursors (X_1) and of the concentration of the photocatalytic system employed in the degradation process (X_2). B_1 is the coefficient of the linear effect of X_1 , B_2 is the coefficient of the linear effect of X_2 , B_{11} is the coefficient of the quadratic effect of X_1 , B_{22} is the coefficient of the quadratic effect of X_2 , B_{12} is the coefficient of the interaction effect between X_1 and X_2 . Significance of coefficients – *: $p < 0.05$; **: $p < 0.01$; ***: $p < 0.001$).



This item was downloaded from IRIS Università di Bologna (<https://cris.unibo.it/>)

When citing, please refer to the published version.

Figure S2. Response surface for the effect of interactions between X_1 and X_2 on the rate to complete photochemical degradation of phenol. X_1 is the rare earth element concentration, X_2 is the photocatalyst concentration in analysed solutions containing phenol. Axes are dimensionless.

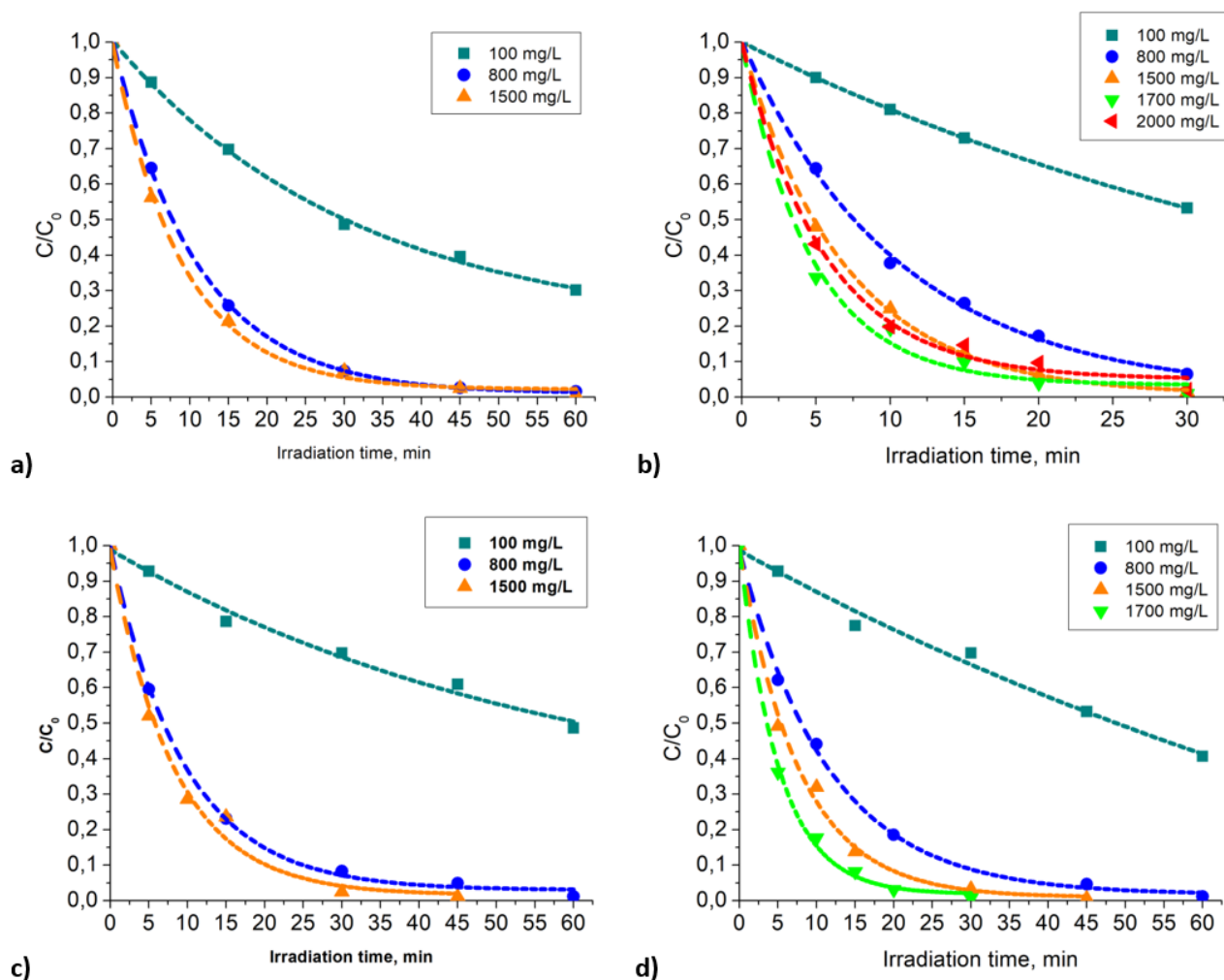


Figure S3. Phenol degradation using the different photocatalysts based on ZnO doped with Cerium: a) CeZn0.5-Cl; b) CeZn1-Cl; c) CeZn0.5-NO₃; d) CeZn1-NO₃.

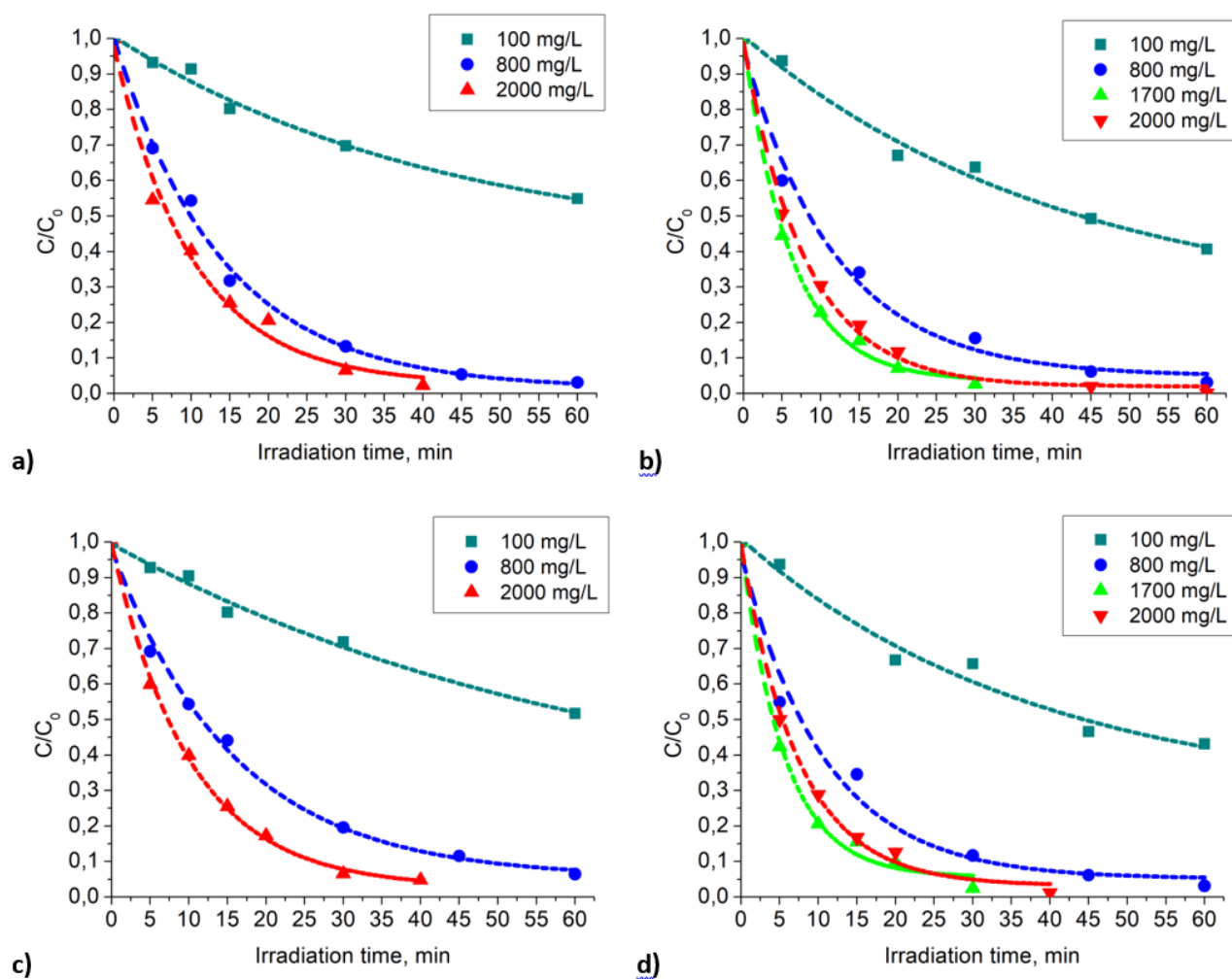


Figure S4. Phenol degradation using the different photocatalysts based on ZnO doped with Erbium: a) ErZn0.5-Cl; b) ErZn1-Cl; c) ErZn0.5-NO₃; d) ErZn1-NO₃.

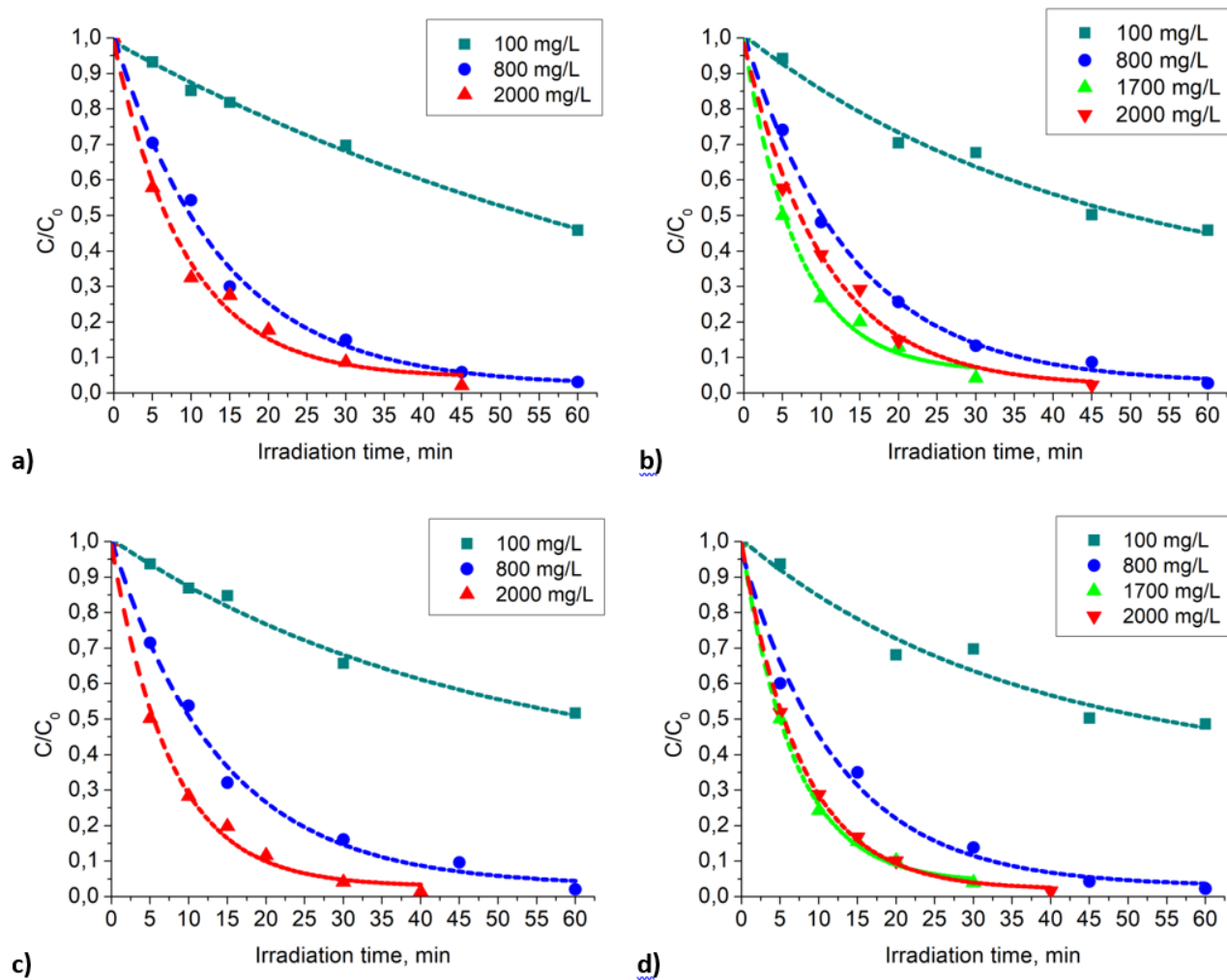


Figure S5. Phenol degradation using the different photocatalysts based on ZnO doped with Ytterbium: a) YbZn0.5-Cl; b) YbZn1-Cl; c) YbZn0.5-NO₃; d) YbZn1-NO₃.

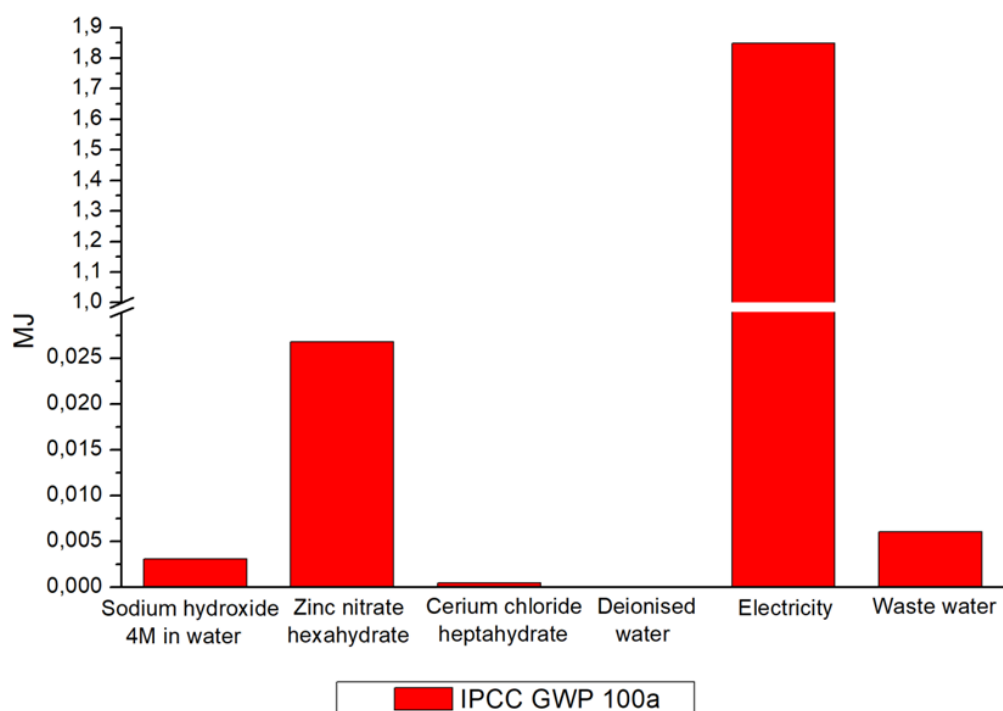


Figure S6. Global Warming Potential IPCC 2013 GWP 100y of the synthesized catalyst: CeZn1-Cl. Output of the synthesis is 1.7 g of photocatalysts.

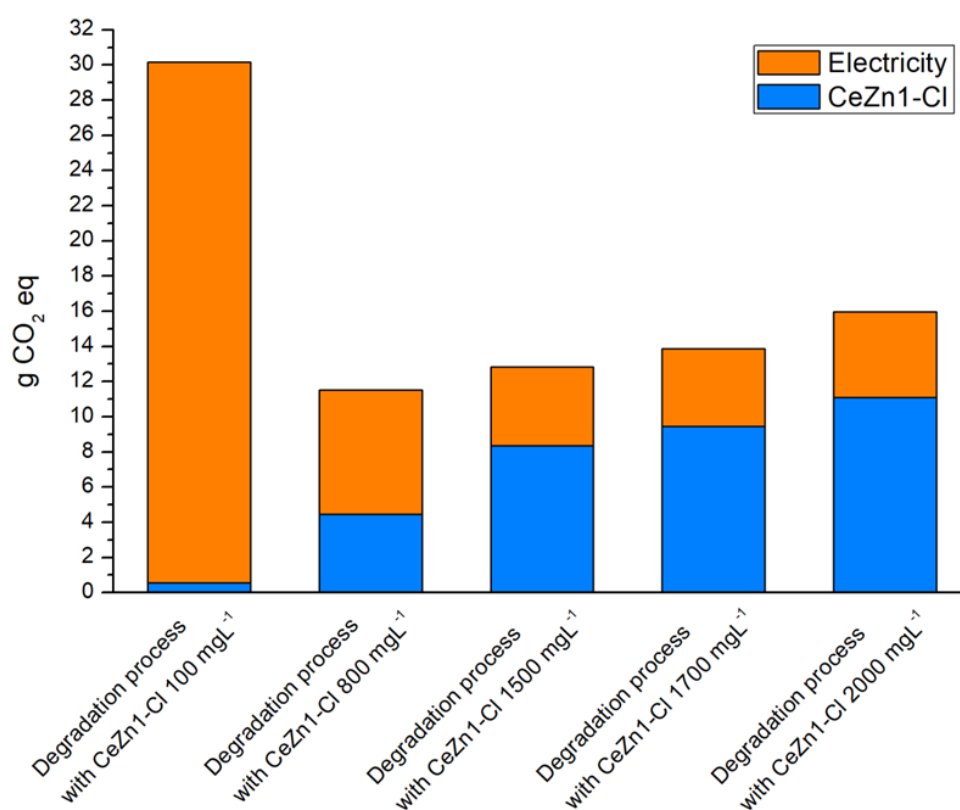


Figure S7. Comparison of the LCIA results for the degradation process using the Global Warming Potential IPCC 2013 GWP 100y (g CO₂ eq) method.